Experimental analysis of separately controlled multi coils on the performance of MR absorber under impact loading

Jiajia Zheng[1], Qing Ouyang[1], Zhaochun Li[2], Yancheng Li[3] and *Jiong Wang[1]

[1]School of Mechanical Engineering, Nanjing University of Science and Technology, Nanjing, China
[2]School of Mechanical Engineering, Nanjing Forestry University, Nanjing, China
[3]School of Civil and Environmental Engineering, University of Technology Sydney, Australia

ABSTRACT: A magnetorheological (MR) absorber is capable of active adapting any gun recoil condition by means of controlled Coulomb force. The objective of multi coils MR absorber with individual input currents is to mitigate the peak force transferred to the buffer structure during bullet firing, and thus to increase the structural fatigue life. This paper investigates various cases by applying random combinations of input currents in the magnetic coils. The impact tests were conducted by obtaining and analyzing the force, displacement, velocity. As a reference, input currents with equivalent magnitude are considered statistically, in terms of average peak force and occurrence time. The experimental results show that separately controlled multi coils contribute to the magnitude and occurrence time of peak force significantly. Furthermore, to reduce peak forces, a simple open-loop control strategy was proposed and validated effectively by the experimental results.

Key words: MR Absorber; Multi-coil; Individual Current; Peak Force;

Introduction

Energy absorption from firing gun requires a gun recoil system to be adaptive due to the uncertainties in the impact payload. Gun recoil absorbers serve to reduce the peak force transformed to the recoil body while limiting its displacement within an allowable range (Wang and Li, 2006; Ahmadian and Norris, 2008; Li and Wang, 2010). A typical hydraulic absorber in a gun recoil system uses the optimized orifice to alter the cross-sectional area of fluid flow along the axial direction of the piston (Balandin et al., 2001). The major disadvantage of the typical hydraulic absorber is that the function and operation of a certain hydraulic absorber cannot be changed once the absorber has been manufactured.

One solution to this problem is to implement semi-active damping using magnetorheological fluid, whose apparent viscosity can be strengthened on the application of magnetic field. Consequently, it provides an adaptive resistance to flow in the form of a controllable yield stress, which can be utilized to build a semi-active MR absorber. Thus the MR absorbers have the potential to adapt their stroke profiles to accommodate the complex conditions of impact loadings (Mao et al., 2007; Browne et al., 2009; Woo et al., 2009). Moreover, the power consumption is relatively low compared to active control and the MR absorber displays good stability (Gerlach et al., 2009).

Up to now, the characteristics of MREA (MR energy absorber) under impact loadings have not been understood clearly. Mao *et al* (2005) focused on the description of a laminar or turbulent flow behavior based on the parallel plates or rectangular duct approximation. The effects due to fluid inertia, minor loss, etc, were also considered to describe the high-speed impact behavior of MREA (Mao et al., 2009). In addition, the fluid compressibility (due to both fluid bulk modulus variations and accumulator pressurization) was experimentally validated to play a more significant role in MREA behavior (Hong et al., 2003; Mao et al., 2013). Though the prior investigations were shown to be able to capture the hysteresis behavior in the force-velocity loop of MREA under impact loadings, the dynamic response (force-time history) of MR absorber under impact loadings still needs further study.

The energy of the impact loading is dissipated by the frictional movement of a piston, which also provides a real-time response for closed-loop control. During compression, the MR fluid is forced to turbulently flow through the active orifice, which provides enforced damping under an applied magnetic field, resulting in undesirable force fluctuations. For instance, peak force can be generated during the early stage of the impact loading. The impact efficiency can be utilized to evaluate the severity of this fluctuation and the most efficient response is featured by rectangular

For Peer Review

force/displacement curve with the lowest possible peak force (Currey, 1988). As attempts to achieve highest impact efficiency, many control strategies have been investigated by the researchers in recent years. Li and Wang (2012) theoretically and experimentally analyzed a full scale gun recoil buffering system which works under real firing impact loading conditions. The results indicate that the optimal control is much better than passive control with smaller variation of the recoil force and less displacement of the recoil body. Singh and Wereley (2013) addressed the non-dimensional analysis and optimal control design of adaptive magnetorheological shock isolation (MRSI) mounts for drop-induced impacts. Two control objectives (stroke and Bingham number) were used to ensure that the payload achieved a soft landing at the end of the compression stroke and the available MREA stroke recovered during rebound. The optimal control of a gun recoil absorber was also investigated for a trade-off between recoil loads minimization and increased rate of fire (Singh HJ and Wereley NM, 2014). In the application of landing gear, two control strategies (semi-active and active) were investigated by Mikulowski and Jankowski (2009) to mitigate the peak force transferred to the aircraft structure. Wang and Carl (1999) proposed the fuzzy logic control for semi-active landing gear system and the numerical results show that it is capable of reducing the maximal structural load. Dong and his co-workers (2013) proposed a human simulated intelligent control (HSIC) to adaptively tune the MR absorber. The results show that HSIC exhibits good adaptive ability and strong robustness under various payloads and sink velocities.

The fundamental goal of the gun recoil system is to utilize the entire stroke to minimize the load transmitted to recoil body during the impact loading (Wereley et al., 2011). The MR absorber designed in this paper has a long stroke (650mm) and is characterized by multi coils to significantly boost the controllability (Gavin, 1998). To take advantage of the long annular duct of the multi-coil MR absorber, the magnetic coils are designed being applied with individual input currents, which means the quantity of working magnetic coils and magnitude of each input currents can be controlled at the same time. To date, the impact of such advantage on the dynamic performance subjected to impact loading is not yet explored. This study focuses on the effects of separately controlled multi coils on the performance of the MR absorber under impact loading. Furthermore, a novel control strategy is proposed and shown to be appropriate for enhancing stability of buffer system (e.g. reducing peak forces and fluctuations) by the experimental tests.

Overview of Experimental set-up

Conceptual Design of Multi-coil MR absorber

Figure 1 displays the schematic diagram of the multi-coil MR absorber. The number of turns for each magnetic coil is 500 with 0.69 mm diameter copper wire. The enameled wires come from the wire-leaded hole 3 and winds around the groove to form four parallel magnetic circuits. There are four wire-leaded holes inside the piston, thus each coil can be applied with input current separately. The magnetic path includes the cylinder, MR fluid and piston head. To guarantee the magnetic flux lines go along the designed path, the piston rod and guide head connecting the piston head are made of aluminum and copper respectively. The specifications of the multi-coil MR absorber are shown in table 1.

Being energized by the magnetic field, the MR absorber can generate controllable Columb force to damp the reciprocation of piston rod by either altering the quantity of working magnetic coils or magnitude of the input currents. Meanwhile, the MR absorber acts as a conventional viscous damper when no input currents are applied on the magnetic coils.

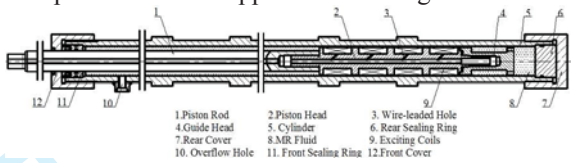

Figure 1 The structure of multi-coil MR absorber

Table 1 Main parameters of the MR absorber

Maximum stroke (mm)	Number of coils	Turns of one coil	Gap width (mm)	Inner diameter of cylinder (mm)	Effective length of piston head (mm)
650	4	500	1.5	40	40

Impact test system

Figure 2 shows the impact test system which is used to investigate the performance of the MR absorber based on separately controlled multi coils. It consists of a host computer, a data acquisition system, a current controller, an impact testing rig and four power supplies. The damper is mounted to the shaft sleeve with recoil mass, and the piston rod is connected to the ground. During the impact test, the explosion of powder in the closed bomb produces a large impulsive force, under which the recoil mass, together with the MR absorber cylinder moves to the right along the guide rail. The elastomeric bumper is designed to provide a buffer for the recoil mass in case that the recoil exceeds the maximum length of 585mm on this rig. The current controller is used to

For Peer Review

control the damping force according to the applied control algorithms.

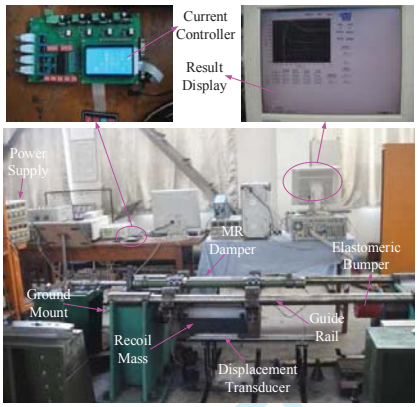

Figure 2 Impact test platform system

Mathematical modeling

The impact test system shown in Figure 2 includes a barrel and a MR absorber and thus can be considered as the single-degree-of-freedom system as shown in Figure 3. The MR absorber connects the barrel with a fixed base, and the recoil mass slides along the axial direction when an impact force acts on the recoil body. The motion of the body is described by the following equation:

$$m_h \frac{d^2X}{dt^2} = F_{pt}(t) - F_R(\dot{x}, B) - F_f \qquad (1)$$

Where m_h is the mass of the recoil body, $F_R(\dot{x}, B)$ is the resistant force produced by the MR absorber, F_f is the friction when the recoil mass moves along the guide rail, and F_{pt} is the impact force due to the explosion of the gunpowder.

The typical impact load F_{pt} caused by the gunpowder has two phases. In the first phase, the gunpowder experiences a very short explosion and the cavity pressure rises sharply; here F_{pt} is proportional to the average pressure inside the chamber. The second phase of F_{pt} begins with the escape of gunpowder gas from the cavity, causing a sharp fall of gas pressure and density; F_{pt} becomes zero quickly with a negative exponential function which has been verified by tests. The second phase can be expressed as follows:

$$F_{pt} = F_g e^{-\frac{t-t_g}{b}} \qquad (2)$$

where t_g is the start moment of the second phase of impact loading, b is a time constant which reflects the declining speed of the impact loading, and

$$F_g = \frac{1}{\varphi}(1 + \frac{1}{2}\frac{\omega}{m})Ap(t_g) \qquad (3)$$

where ω is the mass of the gunpowder, m is the mass of the cylindrical iron, A is the cross area of the cylindrical iron, φ is a coefficient of secondary power and p is the average pressure inside the chamber. Normally, the magnitude of the impact loading due to the explosion of the gunpowder depends on the amount of charge filled in the chamber. In simulation, the impact force from the explosion of gunpowder is usually expressed as a half sinusoidal function combining a negative exponential function,

$$\bar{F}_{pt} = \begin{cases} A\sin(\frac{\pi}{\tau}t) & 0 \le t \le t_g \\ A\sin(\frac{\pi}{\tau}t_g)e^{-(\frac{t-t_g}{b})} & t \ge t_g \end{cases} \qquad (4)$$

where A, τ, and t_g are constants and satisfy the two conditions $A \gg 1$, $t_g \ll$ T(total working time). Figure 4 shows a typical impact loading of regular gunpowder charge versus the time.

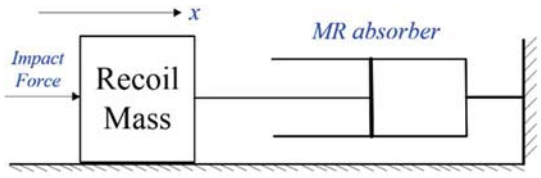

Figure 3 Model of a buffer system with an MR absorber

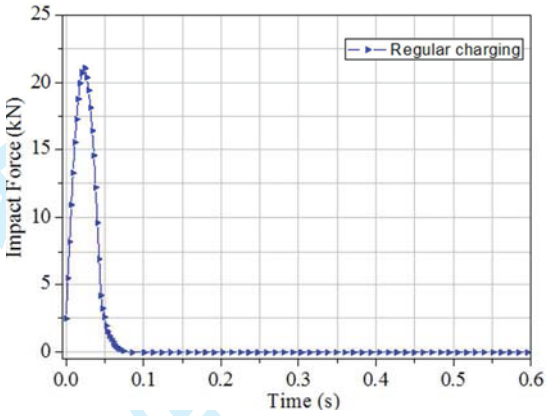

Figure 4 Impact force (A=21.4, τ=5e-2, t_g=4.68e-2, b=9e-3)

In the recoil process, the recoil mass obtains a fast initial velocity v_0 at the time when the impact force starts dropping down to zero. The recoil mass then moves along the axial direction with decreasing velocity until completely stopping. The recoil buffer system is actually an absorber mechanism which aims to transform the impact load F_{pt} with dramatic variation and short duration into a damping force with longer effective time and smaller amplitude.

The key objective of an impact buffer system (e.g. gun recoil system) is to satisfy stability, which requires the dynamic damping force to be smooth without large peak forces. To reduce the maximum peak force, the damping force should be real-time controlled within a permitted displacement (Balandin et al., 2001).

For Peer Review

Results analysis

Figure 5 (a) presents the time history of damping force at different input currents, e.g. 0A, 0.5A, 1A, 2A, when impulse loading impacts the recoil force. It is obvious that the damping force increases when the input current increases due to the strengthened apparent viscosity of MR fluid. The larger damping force leads to less recoil displacement under impact loading, as shown in Figure 5 (b). In the case of input current of 0A, the peak force is 2500N, which is almost half in the case of input current of 2A. Furthermore, it reaches the maximum displacement of 585 mm and then stops by the elastomeric bumper with a reverse displacement of 150 mm. Correspondingly, the velocity of the recoil mass comes to a sudden stop and obtains a backward motion with an initial velocity, as shown in Figure 5 (c). In general, the recoil displacement can be limited within an allowable range. For example, increasing the current may obtain small recoil displacement, but it sharpens the peak damping force, which will definitely cause instability in the buffer system.

Zhang *et al* (2010) indicated that the entire dynamic response of ER absorber was characterized by three distinct stages, namely, an initial shock, a transition stage, and a stable flow stage. In this paper, similar phenomenon was observed based on the experimental results. However, the impact process always experiences the compression of the air before the effect of instant shock appears. Thus the entire impact response of long-stroke MR absorber is featured with four stages, namely, (1) air compression, (2) instant shock, (3) transition stage and (4) flow stage.

In the beginning of the impact, the displacement of the piston increases to 50mm (Figure 5b) while the velocity increases to 2.25 m/s (Figure 5c), while the total force remains unchanged due to the compression of air bubbles inside the MR absorber. In the second stage, the piston starts to push the MR fluid due to the fluid lock (Ahmadian and Norris, 2008). Once the MR fluid starts to flow, the first peak force occurs. However, before the flow, the MR fluid has to overcome the quasi-static yield stress τ_{YS} which is distinguished from the dynamic yield stress τ_{YD}. The constitutive relation of the MR fluid should be expressed by (Zhang et al., 2010):

$$\tau = \begin{cases} G\gamma + \mu_0\dot{\gamma}, & \gamma < \gamma s \\ \tau_{YD} + \mu_0\dot{\gamma}, & \gamma \geq \gamma s \end{cases} \quad (7)$$

$$G = K_t\tau_{YD}/\gamma_S \quad (8)$$

where G is the shear modulus of the MR fluid before yielding, γs is the yield shear strain and K_t is a coefficient.

In the third stage, the flow of MR fluid is resisted by the dynamic yield stress when passing through the long duct. The fluctuations followed by the first peak force are determined by the distribution of the dynamic yield stress along the duct, which will be further discussed in the subsequent sections. After the impact loading, the piston still moves and thus compress the MR fluid. Pressure wave of the MR fluid will hit the end of the cylinder and return back towards the piston. The second peak force occurs when the pressure wave hits the piston head. In the fourth stage, the flow of MR fluid becomes smooth and the resistant force can be calculated as follows:

$$F_R(\dot{x}, B) = A_p \int_0^L (\Delta P_i + k(\Delta P_v + \Delta P_\tau) + \Delta P_m)dx \quad (9)$$

where pressure drops ΔP_i , ΔP_v , ΔP_τ , ΔP_m are generated by the inertia effect, viscous effect, MR effect and minor loss, respectively. The coefficient k depends on the variation of unsteady flow rate.

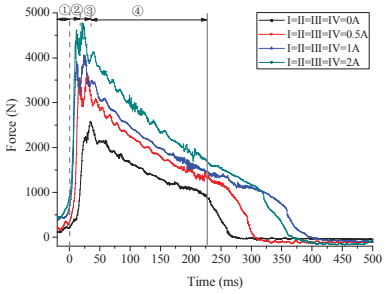

(a)

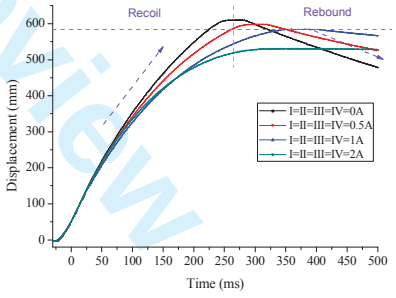

(b)

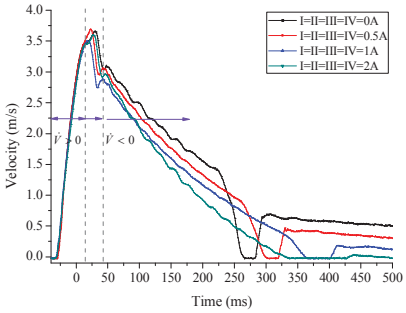

(c)

For Peer Review

Figure 5 Performance of MR absorber: (a) Force (b) Displacement (c) Velocity

Table 2 Cases with different input currents

Cases	**1**	**2**	**3**	**4**	**5**	**6**	**7**
I(A)	2	0	0	0	1	1	1
II(A)	0	2	0	0	1	0	0
III(A)	0	0	2	0	0	1	0
IV(A)	0	0	0	2	0	0	1
Cases	**8**	**9**	**10**	**11**	**12**	**13**	**14**
I(A)	0	0	0	0.67	0.67	0.67	0
II(A)	1	1	0	0.67	0.67	0	0.67
III(A)	1	0	1	0.67	0	0.67	0.67
IV(A)	0	1	1	0	0.67	0.67	0.67
Cases	**15**	**16**	**17**	**18**	**19**	**20**	**21**
I(A)	0.2	0.8	0.3	0.7	0.3	0.7	0.5
II(A)	0.8	0.2	0.4	0.6	0.7	0.3	0.5
III(A)	0.8	0.2	0.6	0.4	0.3	0.7	0.5
IV(A)	0.2	0.8	0.7	0.3	0.7	0.3	0.5

Combinations of applied currents

To analyze the effects of four separately controlled currents on the magnitude and occurrence time of peak force, experimental testing on different cases was conducted under impact loadings. Table 2 shows the 21 cases of experimental testing with different input currents. For example, the case 1 presents the situation when the magnetic coil I is applied with input current of 2A, while other magnetic coils remain off-field. It should be noted that the total input currents in the four magnetic coils are kept as 2A for comparison.

Figures 7-10 show the resultant damping force at different cases. The first peak force F_{p1} occurs at the time T_{p1}, and the second peak force F_{p2} occurs at the time T_{p2}. As can be seen from figure 7(a), the case of coil II=2A induces the largest first peak force F_{p1} with least occurrence time T_{p1}. However, when magnetic coil IV is applied with input current of 2A, the first peak force F_{p1} drops to 3000N and the occurrence time T_{p1} extends to 16.5ms. The case of coil III=2A shows the maximum second peak force to be 4000N, while the minimum second peak force occurs in the case of coil I=2A with 3250N. The above phenomena indicate that the distribution of the yield stress along the gap affects the magnitude and the occurrence time of the peak force. As shown in figure 7(b), the case of increasing yield stress (which is calculated by the FEA based on the characteristics of MR fluid) distributed along the gap (coil IV=2A) obtains smaller first peak force and longer occurrence time. However, the second peak force is enlarged due to the blockage of MR fluid at the end of the long duct. Conversely, the case of decreasing yield stress distributed along the gap (coil I=2A) displays that the first peak force exceeds the second peak force by 300N. Furthermore, the average peak force of the cases of coil II=2A and coil III=2A are larger than that generated by the cases of coil I=2A and coil IV=2A, which represents that the total pressure drop along the duct plays a major role on the average of peak forces.

When two random magnetic coils are applied with each input current of 1A, there are a total of six situations and the results are shown in Figure 8. The distributions of yield stress along the working gap are distinguished according to the overlap and cancellation of magnetic field density in the joint active magnetic poles. Considering the distribution of yield stress along the gap (see figure 8(b)), it is found that the strengthened yield stress produced in the first effective regions reinforces the first peak force F_{p1} and accelerates the occurrence of the first peak force T_{p1}. For example, in the cases of coil II=coil IV=1A, coil II=coil III=1A, coil I=coil III=1A, coil I=coil II=1A, the first peak forces reach 4060N, 3875N, 3850N, 3600N, respectively. While, the first peak times reach 13ms, 12.5ms, 11.5ms, 12ms, respectively. On the contrary, the case of coil III=coil IV =1A shows that the first peak force F_{p1} is 3600N, which is 310N less than the second peak force F_{p2}. While the occurrence time of first and second peak forces are delayed by 2 ms and 3 ms, respectively. The case of coil I=coil IV=1A obtains the minimum peak forces and slows the occurrence of peak times among the six cases of two random working coils.

Figures 9-10 show the cases when three and four magnetic coils are applied with input currents. When coil I=coil III=coil IV=0.67A, minimum first peak force F_{p1} (2800N) and the second peak force F_{p2} (2750N) are obtained because the yield stress is reduced by the cancellation of the magnetic field density among three effective regions. Once the yield stress overlaps in the first three active regions, both peak forces increase as shown in the case of coil I=coil II=coil III=0.67A. Although the distributions of magnetic field density between case of coil I-IV=0.3A:0.4A:0.6A:0.7A and case of coil I-coil IV=0.7A:0.6A:0.4A:0.3A are symmetric, the first case creates a smaller first peak force F_{p1} as well as second peak force F_{p2}. The results are due to the higher yield stress generated in the beginning effective regions enhancing the compression of the MR fluid, which results in larger damping force in the second stage. This also happens in the cases between coil I-coil IV=0.3A:0.7A:0.3A:0.7A and coil I-coil IV=0.7:0.3A:0.7A:0.3A. Thus the dynamic performances of peak forces depend on the magnitude of yield stress as well as the flow direction of MR fluid.

For Peer Review

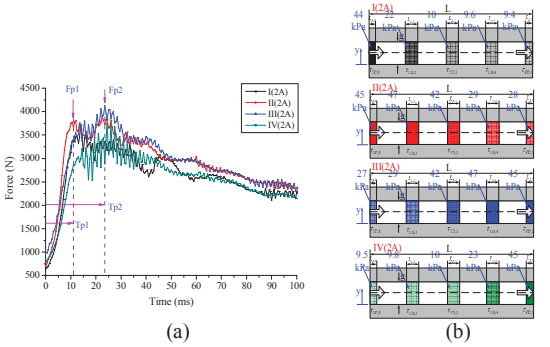

(a) (b)

Figure 7 Cases of one working coil
(a) dynamic response (b) distribution of yield stress along the duct

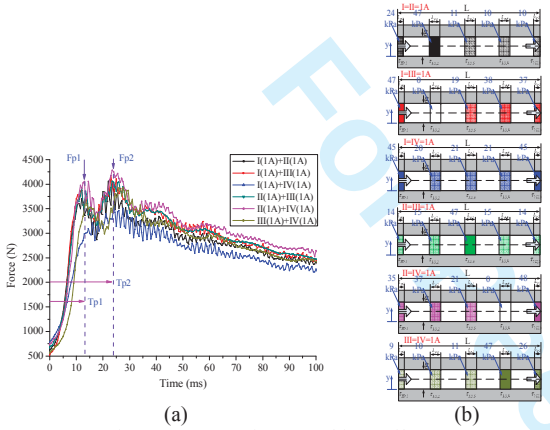

(a) (b)

Figure 8 Cases of two working coils
(a) dynamic response (b) distribution of yield stress along the duct

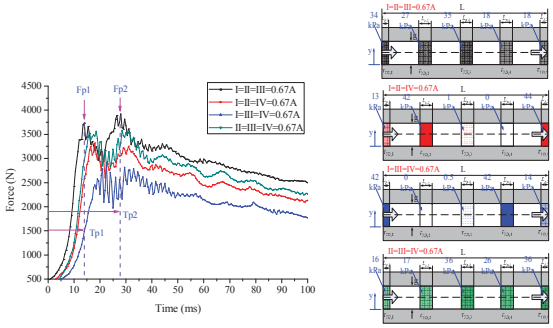

(a) (b)

Figure 9 Cases of three working coils
(a) dynamic response (b) distribution of yield stress along the duct

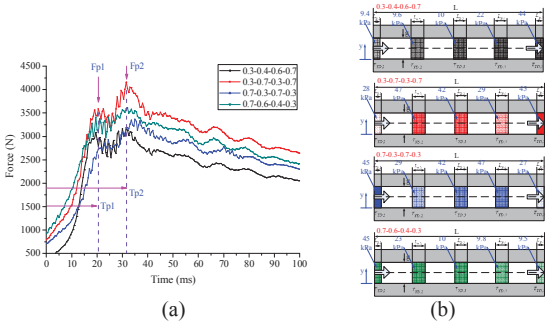

(a) (b)

Figure 10 Cases of four working coils
(a) dynamic response (b) distribution of yield stress along the duct

To conclude, the average peak forces and occurrence times for all cases are shown in figures 11 and 12, respectively. It is clearly observed that the average peak force can be reduced from 4150 N to 2775N by controlling the working coils as well as magnitude of the input currents. Taking the deviation between first peak force F_{p1} and second peak force F_{p2} into account, the case of coil II=coil III=coil IV=0.67A provides the minimum difference, which definitely increases the stability of the buffer system. The occurrence time of the peak force is another important factor that contributes to the stability of the buffer system. The longer first peak time T_{p1} leads to a smaller first peak force $F_{p1}$and vice versa. The case of 0.7-0.3-0.7-0.3 displays the longest occurrence times of both peak force 1 and peak force 2, where corresponding average peak force obtains 3153N, which is suitable in the initialization of control strategy.

For a given impact loading, the smaller damping force means longer damped displacement. The energy consumption during the impact process generated over a period of maximum displacement (585mm) before MR absorber is rebounded by the elastomeric bumper is shown in Figure 13. The four cases of coil I=coil III=1A, coil II=2A, coil I-coil IV=0.2A:0.8:0.8A:0.2A, coil I=2A are better results according to weight ratio between energy consumption and peak force.

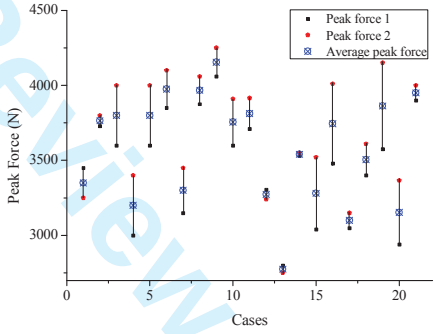

Figure 11 Peak force vs cases

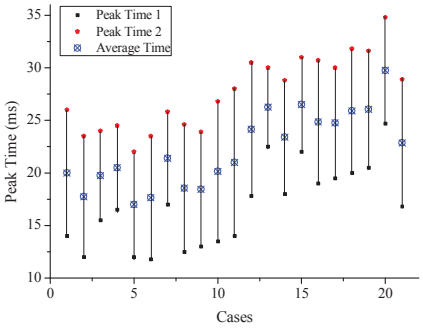

Figure 12 Peak time vs cases

For Peer Review

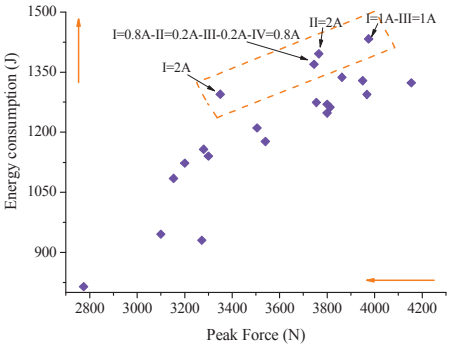

Figure 13 Energy consumption vs peak force

Open-loop Control for the Delayed Peak Forces

Since the dynamic performance of the MR absorber relates to the location of working magnetic coils, a simple open-loop control strategy is presented as shown in Table 3. So far, the open-loop control strategy focuses on the minimized transmission of peak forces to the protected MR buffer system during impact loadings. In general, the impact damping lasts between 500 to 800 ms under current loading conditions. This short time period makes it difficult to implement feedback control strategy effectively as the controller requires certain time to process the feedback and instruct the actuator to respond. The advantage of the proposed strategy (open-loop) makes the damping process more effective without the influence of time delay due to the actuating system [Zheng et al., 2014]. While the development of such control strategy is built upon the understanding of dynamics response of MR absorber as explained above, the open-loop strategy can be applied to general situation of such case.

As can be seen from Figures 7-10, the case with longer axial distance between working magnetic coil (on-state) and inlet of the orifice obtains smaller peak force as well as delayed occurrence time. To mitigate the peak force, the magnetic coils are applied with input currents in the order of coils "IV→IV+III→IV+III+II→IV+III+II+I" and its time interval is chosen as 10 ms so that the damping force can reach its maxima before the impact force ends to zero in order to prevent the MR absorber from bumping into the elastomeric bumper intensively.

Table 2 Open-loop control strategy

Time (ms) \ Magnetic Coil	I	II	III	IV
T_1=0	×	×	×	√
T_2=10	×	×	√	√
T_3=20	×	√	√	√
T_4=30	√	√	√	√

* '×'indicates "off".

'√'indicates "on".

Figure 14 shows the results of the open-loop control strategy on the dynamic performance of the MR absorber under impact loading. It is clearly noted that the peak forces reduce significantly and the occurrence time of peak forces also delays greatly. The discrepancy between the first peak forces ΔF_{p1} (Figure 14a) reaches 300N and the time discrepancy ΔT_{p1} is delayed by 5ms. An expanded discrepancy of ΔF_{p1} is found by increasing the input currents from 0.5 to 2 A (Figure 14b and c). It tends to slow down the occurrence of peak forces. However, the time lag between the two peak forces remains a constant. Therefore, the experimental results prove a potential feasibility of the proposed open-loop control strategy on the MR absorber under impact loading. It should also be noted that the open-loop control strategy takes effect with the sacrifices of slower energy dissipation and longer damping displacement.

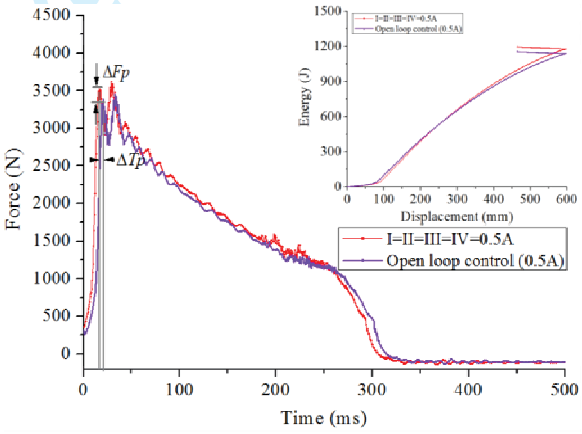

(a)

For Peer Review

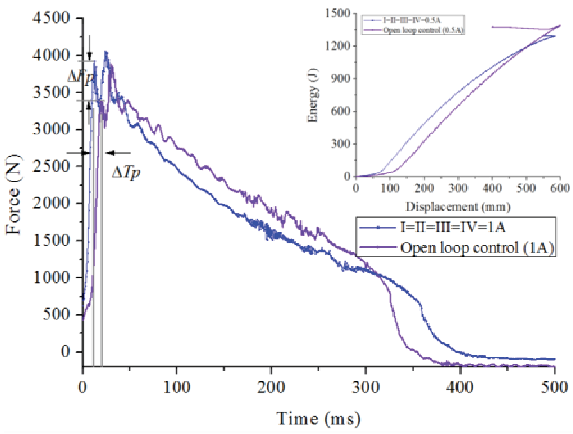

(b)

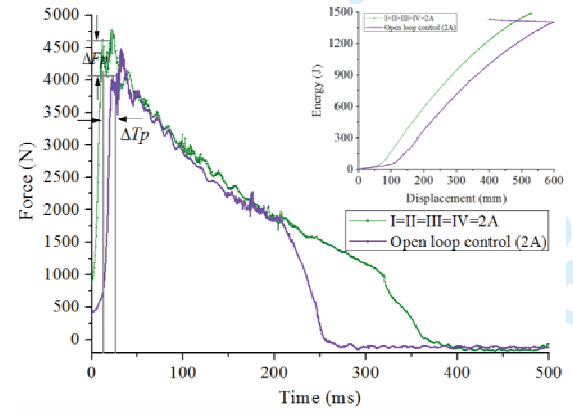

(c)

Figure 14 Effects of open-loop control

Conclusion

Based on the experimental analysis, the effects of separately controlled multi coils on the performance of the MR absorber under impact loading are discussed. It shows that the peak force increases when the input currents increase. To take advantage of the novel conceptual design of the piston head with multiple coils, various cases with individual input currents are investigated to study the magnitude and occurrence time of peak forces. For the multi coils MR absorber, the peak forces transmitted were found to occur at different points relative to the position of working coils used in absorbing the impact. It is believed to be able to decrease the peak forces and shift the occurrence time of the peak force by handling the fluid lock. Thus, 21 cases of applied currents have been tested to investigate the dynamic performance of the MR absorber under impact loadings. Among them, four cases (coil I=coil III=1A, coil II=2A, coil I-coil IV=0.2A:0.8A:0.8A:0.2A, coil I=2A) obtain better results when taking both the energy consumption and peak force into account. Furthermore, to reduce the peak force within limited displacement, it is recommended to apply the magnetic coils from IV to I in order with varied input currents, which was validated by the open-loop control strategy. Further work will further study the open-loop strategy, which achieves the optimal damping force with reasonable peak force and damped displacement in a novel way.

ACKNOWLEGEMENTS

This work was supported by a Natural Science Foundation of China (NSFC) grant funded by the Chinese government. (No.51175265 and No.51305207)

Reference

Ahmadian M and Norris JA (2008) Experimental analysis of magnetorheological dampers when subjected to impact and shock loading Commun. *Nonlinear Sci. Numer. Simul.* 13(9) 1978–85.

Balandin DV, Bolotik NN and Piley WD (2001) Optimal Protection from Impact, Shock, and Vibration (*New York: Gordon and Breach*), CRC Press.

Browne AL, McCleary J, Namuduri CS, et al. (2009) Impact performance of magnetorheological fluids. *J. Intell. Mater. Syst. Struct.* 20 723–8.

Currey NS (1988) Aircraft Landing Gear Design: Principles and Practices, *American Institute of Aeronautics and Astronautics, Inc*.

Dong XM and Xiong GW (2013) Vibration Attenuation of Magnetorheological landing gear system with human simulated intelligent control. *Mathematical Problems in Engineering,* Volume 2013, Aticle ID 242476, 13 pages.

Gavin HP (1998) Design method for high-force electrorheological dampers. *Smart Materials and Structures* 7(5), 664-673.

Gerlach T, Ehrlich J. et al (2009) Novel active vibration absorber with magnetorheological fluid. *Journal of Physics: Conference Series* 149 012049.

Hong SR, Choi SB, Choi YT, et al (2003) Comparison of damping force models for an electrorheological fluid damper. *Int. J. Veh. Des.* 33 17–35.

Li ZC and Wang J (2010) Experiment investigation of magnetorheological damper for high impulsive load. *ASME Conf. Proc. Conf. on Smart Materials, Adaptive Structures and Intelligent Systems.* pp 303–7.

Li ZC and Wang J (2012) A gun recoil system employing a magnetorheological fluid damper. *Smart Mater. Struct* 21 105003.

Mao M, Choi YT and Wereley NM (2005) Effective design strategy for a magnetorheological damper using a nonlinear flow model. *Proc. SPIE* 5760 446–55.

Mao M, Hu W, Choi YT and Wereley NM (2007) A magnetorheological damper with bifold valves for shock and vibration mitigation. *J. Intell. Mater. Syst. Struct* 18 1227–32.

Mao M, Hu W, Wereley NM, et al. (2009) A nonlinear analytical model for magnetorheological energy absorbers under impact conditions. *In ASME 2009 Conference on Smart materials, Adaptive Structures and Intelligent Systems (pp. 393-404), American Society of Mechanical Engineers*.

Mao M, Hu W, Wereley NM, et al. (2013) Nonlinear modeling of magnetorheological energy absorbers under impact conditions. *Smart Mater. Struct.* 22 115015 (12pp).

Mikułowski G and Jankowski L (2009) Adaptive landing gear: optimum control strategy and potential for improvement. *Shock and Vibration 16(2),* pp. 175–194.

Singh HJ and Wereley NM (2013) Adaptive magneto-rheological shock isolation mounts for drop-induced impacts. *Smart Mater. Struct* 22(12) 122001.

Singh HJ and Wereley NM (2014) Optimal control of gun recoil in direct fire using magnetorheological absorbers. *Smart Mater. Struct* 23(5) 055009.

Wang J and Li YC (2006) Dynamic simulation and test verification of MR shock absorber under impact load. *J. Intell. Mater. Syst. Struct* 17 309–14.

Wang XM and Carl U (1999) Fuzzy control of aircraft semiactive landing gear system. In: *Proceedings of the 37th Aerospace Sciences Meeting and Exhibit,* pp: 1–11.

Wereley NM, Choi YT and Singh HJ (2011) Adaptive energy absorbers for drop-induced shock mitigation. *J. Intell. Mater. Syst. Struct* 22 515–9.

Woo D, Choi SB, Choi YT, et al. (2007) Frontal crash mitigation using MR impact damper for controllable bumper. *J. Intell. Mater. Syst. Struct* 18 1227–32.

Zhang XW, Yu TX and Wen WJ (2010) Eletrorheological Cylinders used as Impact Energy Absorbers. *J. Intell. Mater. Syst. Struct* 21(7) 729-745.

Zheng J, Li ZC, Koo J-H, et al. (2014) Analysis and compensation methods for time delays in an impact buffer system based on MR dampers. *J. Intell. Mater. Syst. Struct* 26(6), 690-700.

For Peer Review